References

[1] Ashkenas, I. L., Jex, H. R., and McRuer, D. T., "Pilot-induced oscillations: Their cause and analysis," Northrop Corp., Norair Div., Rept. NOR-64-143 (1964); also Systems Technology Inc., Rept. TR-239-2 (June 20, 1964).

[2] Ashkenas, I. L., "Comment on 'Low-altitude, high-speed handling and riding of volities,' " J. Aircraft **1**, 222–223 (1964); also A'Harrah, R. C., "Reply by author to I. L. Ashkenas," J. Aircraft **1**, 223–224 (1964).

[3] Hirsch, D. L., "Investigation and elimination of PIO tendencies in the Northrop T-38A," Society of Automotive Engineers (July 1964).

[4] Levi, O. A. and Nelson, W. E., "An analytical and flight test approach to the reduction of pilot induced oscillation susceptibility," *AIAA/AFFTC/NASA-FTC Testing of Manned Flight Systems* (American Institute of Aeronautics and Astronautics, New York, 1963), pp. 1–9; also J. Aircraft **1**, 178–184 (1964).

[5] Ashkenas, I. L., and McRuer, D. T., "Optimization of the flight-control, airframe system," J. Aerospace Sci. **27**, 197–218 (1960).

NOV.-DEC. 1966 J. AIRCRAFT VOL. 3, NO. 6

Recent Research Results in the Aerodynamics of Supersonic Vehicles

A. Warner Robins,* Odell A. Morris,† and Roy V. Harris Jr.‡
NASA Langley Research Center, Hampton, Va.

The continuing aerodynamic-research effort aimed at improving the design of supersonic-cruise vehicles has recently produced some significant results. Research by both government and industry has provided, in addition to a better understanding of the design problem itself, some new and very useful design tools and concepts. Some of the advantages of these methods in the treatment of wave drag and drag due to lift are briefly discussed. Also presented are some new considerations of aerodynamic interference and its effect on the aerodynamic efficiency of the trimmed vehicle. An illustrative example of the application of these design tools and concepts to the aerodynamic design of a supersonic-cruise vehicle (SCAT 15-F) is made. A parallel analytic and experimental buildup of the vehicle is presented, including treatment of the symmetric (flat camber-plane), the warped, and the warped-and-reflexed versions of the configuration. The potential of the new techniques is demonstrated by the good agreement between experiment and theory and by the high level of vehicle performance.

Introduction

A BASIC aim of aerodynamic research is to provide the design aerodynamicist with rational, rapid, and reliable means for evaluating the aerodynamics of a given aerodynamic shape and to enable him to assess quickly the cost in aerodynamic efficiency of proposed changes in vehicle shape brought about by other considerations. A short reaction time for the aerodynamicist will permit him to participate more effectively at the vehicle concept stage and thus provide for a more comprehensive design process. Intensive effort by both government and industry therefore has been devoted to the implementation of existing theory with new analytical numerical methods such that the high-speed computer might provide calculative results heretofore restricted to certain relatively simple shapes. Some significant contributions to this end have recently been made. These, along with other new considerations of the aerodynamics of the supersonic vehicle, will be discussed.

Presented as Preprint 65-717 at the AIAA/RAeS/JSASS Design and Technology Meeting, Los Angeles, Calif., November 15–18, 1965; submitted January 13, 1966; revision received June 22, 1966.

* Head, Supersonic Mechanics Section, Full Scale Research Division.

† Aerospace Engineer, Full Scale Research Division.

‡ Aerospace Engineer, Full Scale Research Division. Member AIAA.

Discussion

Zero-Lift Wave Drag

One of the most useful developments has been the application of the high-speed computer to the problem of rapidly determining the zero-lift wave drags of highly complex shapes. Most early efforts aimed at treating the complex case, such as the "transfer rule" of Ward[1] and, of course, supersonic area rule,[2, 3] involved the concept of equivalent bodies of revolution. These efforts had depended upon graphical or semigraphical schemes for generation of the geometry of the many equivalent bodies and utilized, with erratic results, a Fourier series representation of the slopes of areas of these bodies in the drag calculations. More recent schemes[4] accomplish the geometric exercise with the computer using a mathematical model of the aircraft as shown in Fig. 1 and determine the drag of the equivalent bodies as represented by least-drag paths through the computed cross-sectional areas. The result is a significant advancement in both speed and accuracy. The right-hand portion of the figure shows the agreement between calculated and experimental values in the Mach number range from 1.4 to 3.2 for very complex, complete configurations designed for supersonic cruise, varying from fighter-type vehicles on the upper right to bomber and transport types on the left. Except for the three high points, all of which may have resulted from boundary-layer separation, the agreement is generally good. Such computer programs certainly represent a powerful aid to the design aerodynamicist.

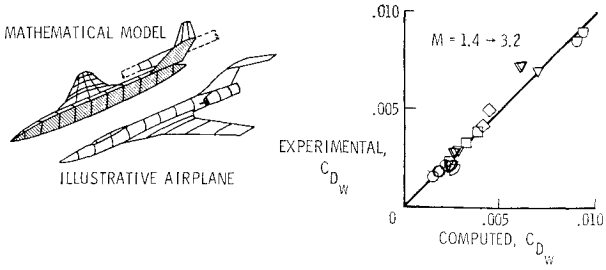

Fig. 1 Zero-lift wave drag.

Design of the Supersonic Wing

Another important application of the high-speed computer to supersonic aerodynamics has removed two rather severe limitations to supersonic wing design. The most obvious restriction eliminated involved wing planform; where once only simple planforms could be readily handled, essentially arbitrary planforms may now be treated.[5, 6] The other limitation was the "inverse" problem; that is, given the wing planform and wing warp, find the load distribution. The ability to define the theoretically optimum wing warp, given the planform and the design lift coefficient, had long since been possible for simple planforms. This last limitation had led to some confusion. Since the theory, as applied to the common arrow wing, for example, called for extreme slopes of the root chord, as seen in Fig. 2, and since these slopes could never be faithfully represented experimentally for obvious reasons, no real check of the theory, as applied to warped wings, could be made. The difference between the theoretical and real wings lay within a small region of the planform near the plane of symmetry and was rather generally thought to be of little consequence. The drag polars on the left in the figure show typical lack of agreement between experiment for the real wing and theory for the theoretical wing. In contrast (but not shown here), experiment and theory generally showed good agreement for the flat wing. The theoretial flat-wing and lower-bound polars are shown here for reference. It should be noted that the lower-bound curve represents the envelope of polars for a family of wings, each having optimum warp for a different lift coefficient. In all of these theoretical polars, of course, no leading-edge suction is assumed. With the removal of the "inverse" restriction, however, the new computer program has enabled, for the first time, the comparison of the theoretical and experimental values for the real wing, as shown on the right. Thus it is seen that the previous disparities were not because the theory had failed to represent the real flow, but rather because we had been failing to represent the shapes prescribed by theory. It is seen that, not only may we compute the loading of a complex wing shape at on-design and off-design conditions,

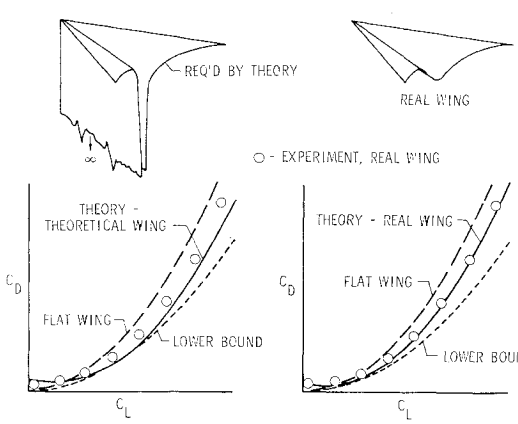

Fig. 2 Drag caused by lift: real and theoretical wings ($C_{L\text{design}}$ = 0.08, Λ = 70°, M = 2.05).

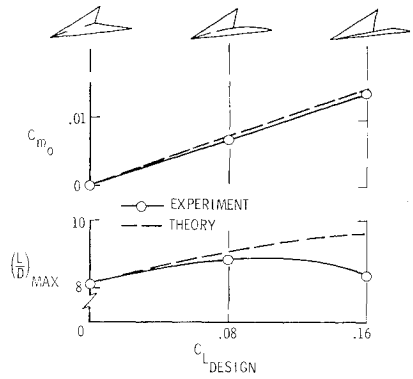

Fig. 3 Effect of wing warp on maximum L/D and zero-lift pitching moment (Λ = 70°, M = 2.05).

but, for reasonable degrees of camber-plane warp, the linear theory on which the computer programs are based may be expected to yield reliable results.

Effects of Wing Warp

There are two characteristics of the warped on twisted and cambered wings which are important to the design aerodynamicist. Generally, the warped wing provides an increment in maximum lift-drag ratio due to improved lifting efficiency and a positive pitching-moment at zero lift (C_{m_0}). This is particularly applicable in the case of the wing with subsonic leading edges. These characteristics are a function of design-lift coefficient (or degree of wing warp), as shown in Fig. 3. Note that at extreme wing design-lift coefficients the theory is unable to represent faithfully the real flow over the highly distorted wing surfaces. Note also that the $C_{L\text{design}}$ = 0.08 wing and the $C_{L\text{design}}$ = 0.16 wing are superior in both respects to the $C_{L\text{design}}$ = 0 or flat wing. These data are from Ref. 7. Figure 4 shows what this means in terms of the maximum trimmed lift-drag ratio, the important airframe flight-efficiency parameter at any given Mach number and stability margin. Here, maximum trimmed lift-drag ratio is plotted as a function of stability margin for wing-body combinations, which, except that one has a flat and the other a warped wing camber plane, are otherwise identical. The important thing to note here is not so much the difference between the maximum lift-drag ratio (between points A and B) as seen in the previous figure but the difference, because of the pitching moment increment, in maximum trimmed lift-drag ratios at some reasonable level of positive stability (between points A and C). This will be noted again later.

Supersonic Aerodynamic Interference

It is certain that the designer of the efficient supersonic-cruise vehicle cannot settle for the thin-element or zero-inter-

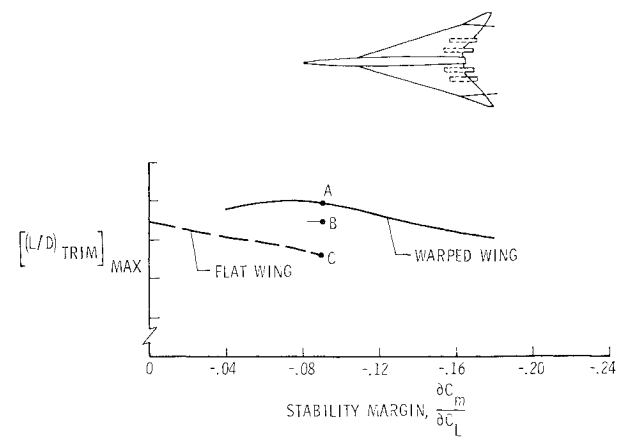

Fig. 4 Effect of wing warp on trim characteristics (M = 2.6).

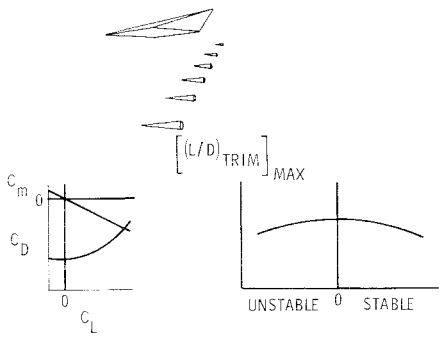

Fig. 5 Interference considerations, symmetric noninterference case.

ference case; the configuration must fit together in such a way that the drag of the aggregate is substantially less than that of the isolated components. Put another way, the avoidance of adverse interference will not be good enough. Because it is not known to be treated adequately elsewhere, much of the remainder of this paper will deal with this subject. The absence of systematic data requires a qualitative treatment using simple, rather obvious examples. The next series of figures, then, will be concerned with interference between components consisting of a double-wedge-section wing semispan and several cones that might be considered equivalent-body representations of engine nacelles.

Figure 5 represents the no-interference case; disturbances produced by any component are not felt by any other component. Representative variations of pitching-moment and drag coefficients with lift coefficient and of maximum trimmed lift-drag ratio with longitudinal stability are shown in the lower portion of the figure. In Fig. 6, the components are arranged so that the compressions from the cones fall upon the receding slopes of the wing and the expansions from the wing impinge upon the advancing portions of the cones. Here the components are helping one another along. This favorable drag interference is reflected in the drag polars at bottom left, where the curves from the previous no-interference case are represented by the dashed lines, and the present case with the solid lines. The compressions from the cones also impose an interference lift along the aft portions of the wing so that a nose-down or negative pitching-moment increment is present, as shown in the curves at lower left. Note that in the limit and neglecting viscous forces the arrangement of components shown in this figure might be represented by the wing with the attached wedge as shown in the sketch at right, and that this is a trailing-edge-down condition. Thus, maximum trimmed lift-drag ratio occurs in the unstable region, and considerable control deflection might be required for trimmed flight at positive stability. In fact, depending on the type of longitudinal controls, it is very possible that this favorable-interference case might be less efficient at reasonable stability levels than the zero-interference arrangement, as is shown on the lower right. Figure 7 represents a favorable-interference case in which wing reflex has been employed. The characteristics of the two previous cases are shown as broken lines and are compared with the solid lines of the present case in the lower part of the figure. First, however, the configuration sketch should be examined. Note that the airfoil is no longer symmetric; that, as noted previously, the airfoil has been reflexed, providing a steeper lower-surface slope that facilitates drag cancellation between the lower surface and the cones; and that the wing upper-surface slope is reduced, lowering its pressure drag. Again note the sketch of the approximately equivalent configuration on the right. Note that, with the wing reflexed and the cones represented by the attached wedge, the result is a symmetric slab-trailing-edge wing that has a still lower drag than the previous or trailing-edge-down arrangement and a pitching-moment curve such as that of the original, no-interference case. Of interest is the fact that a wing thus reflexed approaches the case of an unreflexed, transparent wing in which perturbations from an interference source on one side of the wing are able to pass freely through the wing, affecting pressures on both upper and lower surfaces. This, incidentally, is the way the wave-drag computer program sees it and is why the combination of a reflexed wing and its interference body may be adequately represented to the computer by the geometry of the unreflexed wing and the interference body. It is also interesting to note that wing reflex that is designed to accommodate an interference body in the presence of an "optimum" wing can cancel the lift interference due to that body, preserving the lift distribution originally designed into the unreflexed wing. In any event, referring to the lower right in Fig. 7, the slightly lower drag and the cancellation of the adverse pitching-moment interference provide that the maximum trimmed lift-drag ratio of the arrangement with favorable interference, and wing reflex can be substantially superior to the other two at reasonable levels of stability.

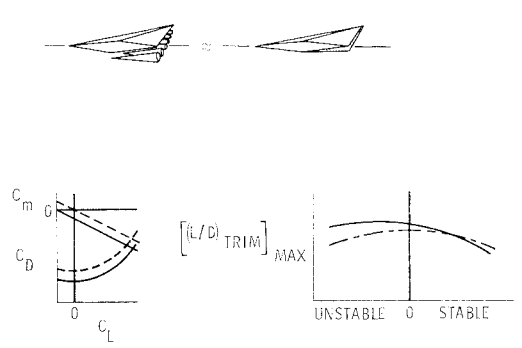

Fig. 6 Interference considerations, favorable interference, unreflexed-wing case.

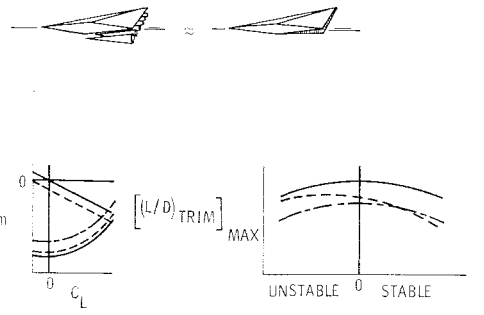

Fig. 7 Interference considerations; favorable interference, reflexed wing case.

Figure 8 provides a review of the previous discussion of interference and relates it to the earlier consideration of wing warp. Progress in the use of interference can be traced from

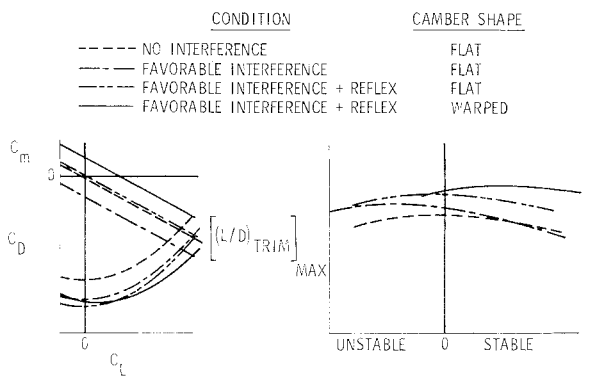

Fig. 8 Interference considerations.

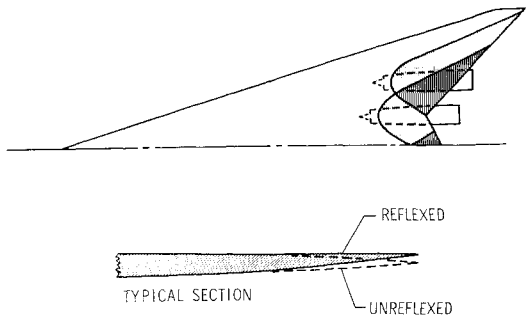

Fig. 9 Wing reflex to accommodate nacelle interference.

zero interference, through favorable interference, to favorable interference with wing reflex. Recalling now that the warped wing can provide lower drag at lift and a positive increment in pitching moment as shown here, application of the favorable interference with wing reflex to the warped wing can provide, at reasonable stability margins, a very large gain in maximum trimmed lift-drag ratio. Thus it is seen that favorable interference can provide improvements in maximum lift-drag ratio while producing decrements in our airframe flight-efficiency parameter at normal stability levels, but that with proper application (including wing reflex) substantial over-all benefits can be realized.

The actual application of wing reflex in order to accommodate nacelle interference might be as shown in Fig. 9. The regions of influence of the nacelles depend primarily on Mach number and lift coefficient and may be satisfactorily defined using nacelle geometry or nacelle equivalent-body geometry and a number of calculative methods, including the method of characteristics, Whitham's modified linear theory, or the cone tables. The interference pressures may be calculated satisfactorily using either of these theories, or an empirical scheme accounting for the total interference lift might be used. Calculation of the slope changes necessary to relieve the wing of the interference pressures, where these pressures are provided in detail, will oftentimes result in steep local slopes, which, even if the theory perfectly matches the real flows, will operate correctly at the one design Mach number and lift coefficient. A reflex shape falling somewhere between this theoretical one and one that results from a linear reflex designed to cancel the total, not the local, interference load will probably be satisfactory. A typical section through the reflexed region of the wing might be as shown at the bottom of the figure.

Effects of Sidewash

Another effect of the installation on the wing of bodies such as nacelles or stores, or of struts, fences, or fins is shown in Fig. 10. The bodies are shown with "toe-in" out of consideration of the sidewash beneath the lifting wing at design condition. The high drag increment at the negative-lift condition comes from the rather extreme misalignment of the bodies, thus oriented, with the underwing sidewash. At some positive lift coefficient they become essentially aligned with the flow, and, at slightly higher values, some thrust component of the body side-force might be generated. A very simple analysis, which neglects body volume effects and the interference of the pressure fields associated with the body-sidewash misalignment, would have the body set at half the local sidewash angle. In any event, it should be remembered, particularly when examining the drag polar of a complex configuration, that, as lift coefficient is changed, dramatic changes in the drag increment due to nacelles, stores, fins, and the like can occur. These effects should not be confused with those of the interference previously discussed.

Sample Application

Figure 11 shows an aircraft configuration that was designed, using the several previously discussed tools and concepts, with a view to focusing attention on these developments. The configuration, supersonic cruise air transport (SCAT) 15-F, nominally represents a long-range supersonic transport vehicle having a cruise Mach number near 2.7. In the generation of the configuration, certain fundamental points, in accordance with the foregoing discussions, seemed apparent. It appeared that the wing-fuseage-nacelles combination should be self-trimming and that the drag due to lift should be lower than the flat plate value (these points, of course, are interrelated.) Furthermore, the components of the configuration should go together so as to provide, as previously noted, for maximum beneficial interference; and, more fundamentally, those components should either lift or thrust or, if not altogether eliminated, at least be minimized. These considerations tended to lead to a configuration having a largely subsonic leading edge and some trailing edge notch, the latter so as to reduce the low-grade lifting surface falling in the downwash of the remainder of the wing. Also, such requirements tend to lead to a warped wing so as to provide the least drag in trimmed flight at the design point. The interference considerations virtually dictated that the engine nacelles be located beneath and rearward on the wing. The minimization of nonlifting or nonthrusting surfaces eliminated the separate horizontal tail and provided that the vertical fins be placed outboard, as shown, in a region of high effectiveness. Thus, the basic concept was set. It remained to exercise the concept analytically so as to establish the trade sensitivities necessary to optimize the aerodynamic shape.

Although the shaping of the configuration with the use of the aforementioned analytic tools and concepts was generally rather straightforward, one particular consideration in the process which has not been previously mentioned is worthy of note. This has to do with integration of the wing-fuselage combination and involves the elimination of fuselage forebody lift and the consequent viscous crossflow on that forebody at design-lift conditions. Such crossflow tends greatly to exceed the design values of local upwash at the wing-root leading edge, a matter of great importance, since the lifting efficiency of the wing is critically dependent for the establishment and spanwise growth of the proper upwash along the wing leading edge, upon achieving correct upwash at the wing root. This being the case, the wing planform considered when calculating the optimum wing warp had to have a blunted apex (since we have said that the forebody, which contains the basic arrow-shaped apex, may carry no lift and, hence, should be neglected). The actual apex selected was parabolic, with the required forebody droop initiating at its origin.

Once the configuration geometry was defined, three wind-tunnel models were constructed. One of these, of course, represented the complete configuration with a warped and reflexed wing, engine nacelles, and vertical tails. The other

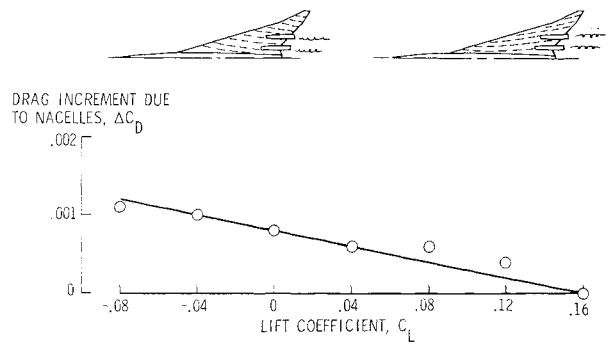

Fig. 10 Effect of lift on nacelle drag increment.

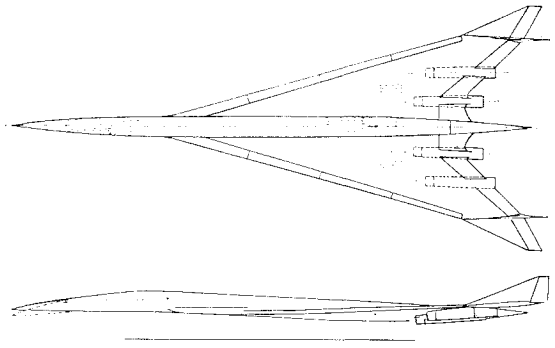

Fig. 11 SCAT 15-F configuration.

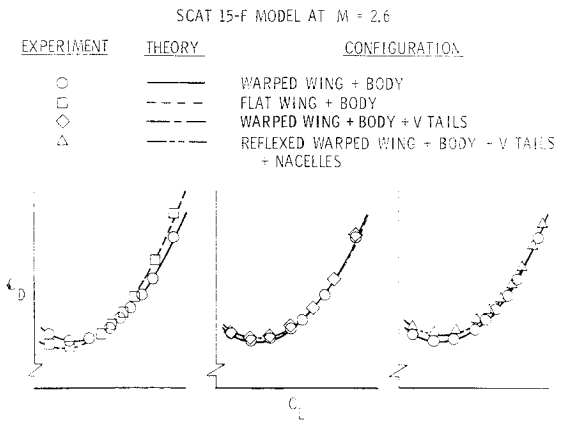

Fig. 12 Experimental and theoretical drag buildup (SCAT 15-F model at $M = 2.6$).

two were designed to provide, with the first, a complete, step-by-step, experimental buildup as set forth in the foregoing discussions. They were, therefore, a wing-body configuration having a flat camber plane and a wing-body combination with a wing warp identical to the complete configuration except that no wing reflex was employed. The results of the analytic and experimental tests are shown in Fig. 12. No pitching-moment data are shown here, the important comparison in this regard having been shown in Fig. 4, which contained data from the tests from which these data are taken and demonstrated the significant benefits of wing warp. This figure traces, in terms of lift-drag polars, the evolution of the configuration through the flat wing-body combination, the warped wing-body configuration with vertical tails, to the complete configuration with its reflexed, warped wing. The reference drag polar is that of the warped wing-body combination, which represents essentially the best that can be done with the configuration without nacelles and vertical tails. In the comparison on the left, the warped wing is seen to be superior, as expected, to the flat wing; although, as noted previously, the most significant benefit of the wing warp is seen in trimmed lift-drag ratio (Fig. 4). In the middle figure, the addition of the vertical tails is seen to produce very little, if any, drag penalty at lift, as would be indicated by earlier discussion. In the right-hand figure, the addition of the vertical surfaces and the four engine nacelles with wing reflex is seen to produce a considerable drag decrement near zero lift which diminishes as lift increases. It is interesting to note that, in addition to the trimming advantages noted earlier, the drag of the complete configuration with all of its components is less than that of the flat-wing-body combination alone at and above the cruise lift. The agreement between theory and experiment for the complete configuration is not as good as that of the others, partially because, no doubt, the theory, although it accounts for the drag due to sidewash of the nacelles and tails themselves, does not account for the distortion of the lift distribution caused by the pressure fields associated with the lateral loads on these components. The over-all agreement between experiment and theory, however, is very good, which, when coupled with the fact that very high lift-drag ratios were attained, attests to the usefulness and soundness of the analytic processes and concepts used.

Summary

In summary, some very useful, well-implemented analytic processes have been developed which promise greatly to improve the speed and reliability with which the supersonic aerodynamics of a configuration may be evaluated. Application of these processes in conjunction with proper treatment of component interference should lead to substantial improvements in the performance of supersonic-cruise vehicles.

References

[1] Ward, G. N., "The drag of source distributions in linearized supersonic flow," College of Aeronautics, Rept. 88 (February 1955).

[2] Jones, R. T., "Theory of wing-body drag at supersonic speeds," NACA Rept. 1284 (1956); supersedes NACA RM A53H18a.

[3] Whitcomb, R. T. and Sevier, J. R., Jr., "A supersonic area rule and an application to the design of a wing-body combination with high lift-drag ratios," NASA TR R-72 (1960); supersedes NACA RM L53H31a.

[4] Harris, R. V., Jr., "An analysis and correlation of aircraft wave drag," NASA TM X-947 (March 1964).

[5] Middleton, W. D. and Carlson, H. W., "A numerical method for calculating the flat-plate pressure distributions on supersonic wings of arbitrary planform," NASA TN D-2570 (January 1965).

[6] Carlson, H. W. and Middleton, W. D., "A numerical method for the design of camber surfaces of supersonic wings with arbitrary planforms," NASA TN D-2341 (June 1964).

[7] Carlson, H. W., "Aerodynamic characteristics at Mach number 2.05 of a series of highly swept arrow wings employing various degrees of twist and camber," NASA TM X-332 (1960).